Original Research Paper

IJES *Iranian Journal of Earth Sciences*
Vol. 14, No. 2, 2022, 131-139.
DOI: 10.30495/ ijes.2021.685387

Identification of Fe^{3+} content in Epidote from Varan, Urumieh-Dokhtar magmatic arc, Iran: using FTIR and Raman spectroscopy

Ghosoun Zheira[1], Fariborz Masoudi[1], Bahman Rahimzadeh[1]

1. Department of Minerals & Groundwater Resources, Faculty of Earth Sciences, Shahid Beheshti University, Tehran, Iran

Received 1 March 2021; accepted 5 September 2021

Abstract

This study is aimed to determine the Fe content in natural epidote from Varan area (Urumieh-Dokhtar Magmatic Arc, Iran) by using vibrational FTIR and Raman spectroscopy and EPMA analyses. Fe^{3+} concentration calculated from FTIR spectroscopic data is in the range of 0.96 to 1 apfu. The results are in complete agreement with EPMA data. The comparison between obtained Raman spectra of studied epidote grains and those from the RRUFF database suggest that epidote from Varan area is rich in Fe^{3+}. High Fe^{3+} content might reflect moderate to high oxygen fugacity during the crystallization of epidote. This short paper demonstrates that the quantification of the Fe content in epidote via FTIR method is as good as EPMA, whereas the utilization of a low-cost Raman spectrometer helps in quickly distinguishing between Fe-rich and Fe-poor epidote, which even could be useful in the case of field studies.

Keywords: *Epidote, FTIR, Raman spectroscopy, Urumieh-Dokhtar Magmatic Arc, Iran.*

1. Introduction

Epidote minerals contain chains of edge-sharing octahedra of two kinds. The first one represents simple edge-sharing chains of M2 octahedra cross-linked by SiO_4 and Si_2O_7 groups (where H atoms are attached to the O atoms) to the second kind of edge-sharing chain of central M1 and peripheral M3 octahedra (Deer et al. 2013, Fig. 1a and 1b). Epidote belongs to the disilicate or sorosilicate structural family containing an isolated silica tetrahedron $[SiO_4]^{4-}$ and corner-sharing pairs of Si tetrahedra $[Si_2O_7]^{6-}$ (Franz and Liebscher 2004; Gieré and Sorensen 2004). Epidote is monoclinic, space group $P2_1/m$ (Yavuz and Yıldırım 2018). The general formula of the epidote group is written as $A_2M_3[T_2O_7][TO_4](O,F)(OH,O)$ or more clearly as A1A2M1M2M3(SiO_4)(Si_2O_7)O4(O10) in which A1 = Ca, Mn^{2+}; A2 = Ca, REE , Sr, Pb, Th; M1 = Al, Fe^{3+}, V^{3+}, Mn^{3+}, Cr^{3+}; M2 = Al; M3 = Al, Fe^{3+}, V^{3+}, Mn^{3+}, Cr^{3+}, Mg, Fe^{2+}, Mn^{2+}; O4=O or F; O10= OH or O (Armbruster et al. 2006). Based on the dominant cations at A1, A2, M1, M2, M3, as well as anions at O4 and O10 sites, three subgroups of epidote are derived from the end-members clinozoisite, allanite, and dollaseite, respectively, as laid down in the IMA (International Mineralogical Association) report by Armbruster et al. (2006). However, the discovery of a new epidote supergroup mineral åskagenite-(Nd) by Chukanov et al. (2010) changed the number of subgroups to four. Epidote-supergroup minerals, with complex solid solutions series, occur in a wide variety of parageneses including magmatic and low to high grade metamorphic rocks, pegmatites, hydrothermal and metasomatic rocks, as well as in many ore deposit types.

---

*Corresponding author.
E-mail address (es): b_rahimzadeh@sbu.ac.ir

Thus, the knowledge of epidote crystal chemistry is essential for applying thermodynamics to understand the conditions of rock formation. In addition, understanding of the genesis, evolution, and interaction of epidotes with the host rock can improve current petrological and geochemical models (Freiberger et al. 2001; Klemd 2004; Campos-Alvarez et al. 2010; Ferreira et al. 2011; Pandit et al. 2014; McFarlane 2016, Sarem et al. 2021). However, the crystal-chemical formula of an epidote specimens is commonly calculated from electron probe micro analyses (EPMA). In recent years, vibrational spectroscopy (e.g., Raman and infrared spectroscopy) have been used as a powerful tool to characterize mineral species from the epidote family.

There are several publications, in which the FTIR (Fourier-transform infrared spectra) and Raman spectra have been used to fingerprint epidote species (Mingsheng and Dien 1987; Perseil 1987; Janeczek and Sachanbinski 1989; Gavorkyan 1990; Petrusenko et al. 1992; Huang 1999; Makreski et al., 2007; Čobić 2015; Varlamov et al. 2019; Yazdi et al. 2022) and attempts have been made to establish a correlation between the framework spectral features and the chemical composition of epidote species (e.g., Langer and Raith, 1974). Major topics of infrared spectroscopic studies have been the OH environment and its changes with composition (Langer and Raith 1974; Della Ventura et al. 1996; Bina et al. 2020). However, a detailed and systematic Raman-scattering study of the OH-stretching range with several samples of different epidote subgroups and complex chemistry, like that performed by using FTIR, is still missing. Indeed, it is well known that the Fe^{3+} content in the members of the clinozoisite-epidote series can be determined via FTIR spectroscopy in the OH stretching spectral range, because the position

of the peak related to the OH-stretching vibrations correlates linearly with the Fe^{3+} content in the M3 octahedral site (Langer and Raith 1974). Clinozoisite and epidote are end members of the Al-Fe^{3+} solid solution series. According to Armbruster et al. (2006), the main difference of epidote and clinozoisite is the Fe^{3+} content at the M3 octahedral site. If the dominant cation at M3 site is Fe^{3+} with $X_{Ep} > 50\%$, the sample is names epidote. The M1 and M2 octahedral sites contain only Al whereas A1 and A2 are most commonly occupied by Ca and possibly Sr. The present study deals with natural epidote from the Varan igneous complex rock units, based on combined Raman and FTIR spectroscopic observation. The quantitative Fe^{3+} content in epidote is determined on the basis of its FTIR and is compared to that derived from EPMA. Also, the potential of Raman compared to those established methods is tested.

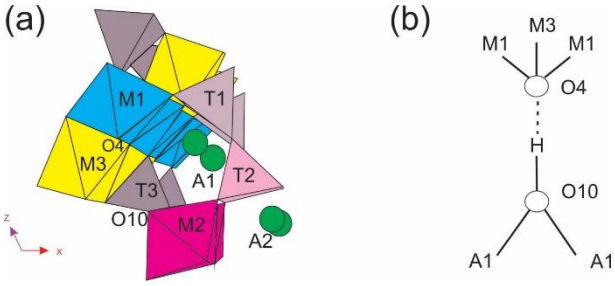

Fig. 1. (a) Polyhedral model of the epidote structure projected along the y axis (Deer et al. 2013); (b) Schematic structural of the OH environment in monoclinic epidote (Della Ventura et al. 1996).

2. Sample description

The epidote was collected from Varan area in the central part of Urumieh-Dokhtar Magmatic Arc (UDMA) of Iran (Fig. 2a). Varan area is located at 60 km South of Qom city. Three major geological units characterize this area from oldest to newest in geological age: 1) Eocene volcano-sedimentary rocks; 2) Qom formation that is composed of marine limestone and marl sediments; 3) the Miocene subvolcanic and intrusive rocks (Fig. 2b). Locally, the contact of intermediate-acidic intrusive rocks with Eocene volcanic-sedimentary successions is distinguished by the effect of hydrothermal fluids due to intrusive emplacement. Fe mineralization and epidotization occurred at the contact with Eocene volcanic-sedimentary units (Fig. 3a). Epidote association with major Fe-oxide minerals suggest that it equilibrated with the mineralizing ore fluids. Magnetite is dominant ore mineral phases in the Varan area whereas hematite Chalcopyrite and pyrite occur as minor phases (Khademi Parsa 2017). In microscopic studies, epidotes show variable strong interference colors (green to pinkish-yellow) and occur as anhedral crystals with size varying from 0.5-2.5 mm (Fig. 3b).

3. Methods

3.1. Electron probe Micro analyses

One selected polished thin section was prepared (K-14) and nine points from three crystals have been analyzed by EPMA method (Table 1). Quantitative electron probe micro analysis of epidote were performed by a Cameca SX100 electron microprobe at the Iran Minerals Processing Research Center, Iran. During operation, accelerating voltage, beam current and beam diameter were 20 kV, 20 µA and 5 µm, respectively.

3.2. Raman spectroscopy

The epidote was carefully picked under a microscope from crashed ore sample and then Raman and FTIR investigations were performed.

The Raman spectra of epidote were recorded using a Takram P50C0R10 Raman Microscope equipped with a Hamamatsu detector at the gemology Laboratory of Shahid Beheshti University. An Nd:YAG laser (λ = 532 nm, Laser Power = 100 mW) was used to excite the Raman scattering. The system was calibrated using the 520.5 cm^{-1} Raman band of silicon. The spectral resolution was ~6 cm^{-1}. The laser radiation was focused to a spot diameter of 14 µm by a 60× upright microscope objective on the selected crystals. The measurements were carried out at room temperature. For the range of 200–1200 cm^{-1}, background correction and peak fitting operations have been performed by using mixed (Gaussian + Lorentzian) functions, using origin software. In the present study, Raman spectroscopy is applied to epidote grains. Two epidote grains investigated by Raman spectroscopy and two representative collected spectra presented. The spectra were collected in random crystallographic orientations.

3.3. FTIR spectroscopy

The infrared spectra were collected with a Bomem MB 102 FT-IR spectrometer with a spectral resolution of 3 cm^{-1} and the spectral range from 400–4000 cm^{-1} at the Shahid Beheshti University in Tehran, Iran. The measurements were taken at room temperature, using the KBr pellet method (with a mineral/KBr ratio of 0.5/150 mg). Since we are dealing with broad bands over a wide spectral range, the spectra-fitting procedure was not used and the raw FTIR spectra are interpreted in the present study.

4. Results and discussion

4.1. Chemical composition

The epidote type was determined based on the Commission on New Minerals and Mineral Names (CNMMN) of the International Mineralogical Association (IMA-2006) nomenclature scheme (Armbruster et al. 2006; Baratian et al. 2018), using the WinEpclas program of Yavuz and Yıldırım (2018) as presented in Table 1.

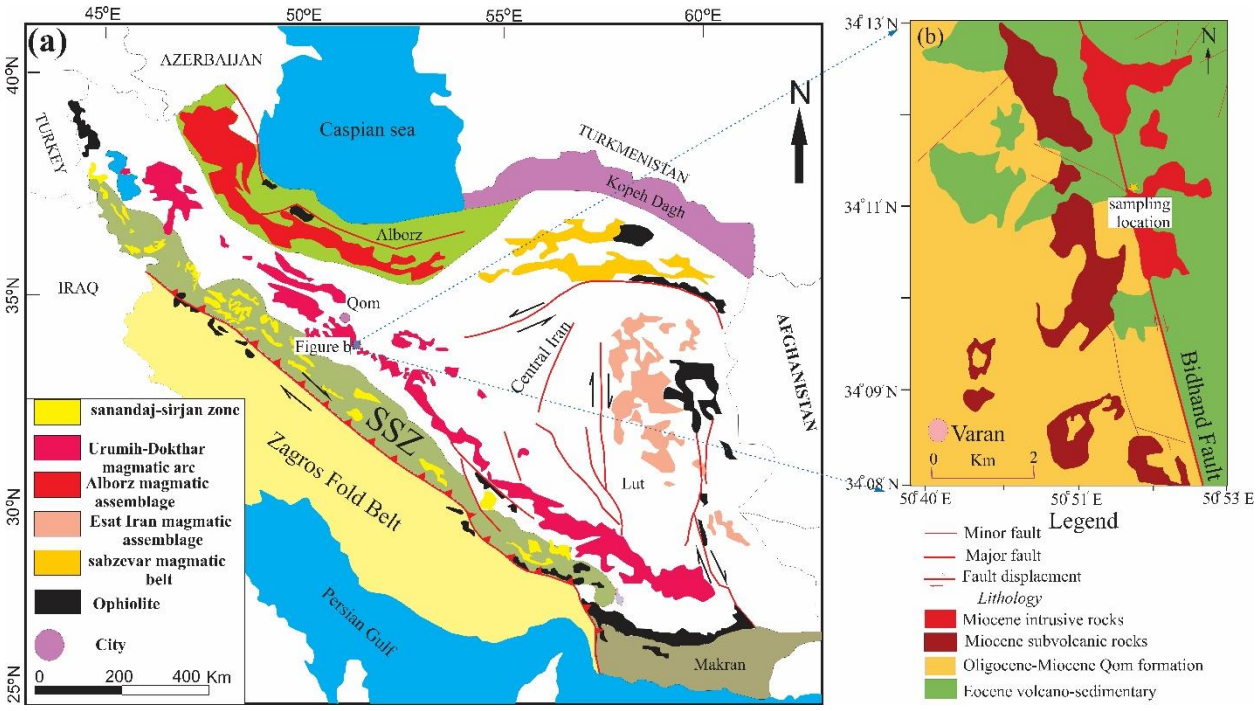

Fig. 2. (a) Simplified geological map of Iran, showing major tectonic units (modified after Alavi 1994); (b) Simplified geological map of Varan area (modified after Ghalamghash and Babakhani 1996).

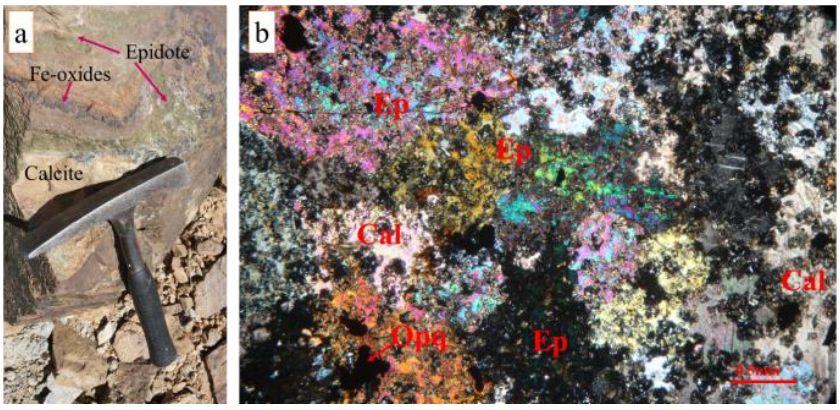

Fig. 3. (a) The occurrence of Fe mineralization and epidotization in contact between Miocene intrusive rocks and Eocene volcanic-sedimentary successions; (b) anhedral epidote with opaque minerals and calcite. Mineral abbreviations based on Whitney and Evans (2010): Ep, epidote; Cal, calcite; Opq, opaque minerals.

The EPMA results of epidote indicate that Al occurs as dominant cation in the M1 and M2 octahedral sites with concentration of 1.93-2.0 apfu whereas the M3 octahedral site is dominated by Fe^{3+}. Fe^{3+} content in the examined epidote varies from 0.886 to 1.0 apfu (Mean: 0.958). A1 and A2 are most commonly occupied by Ca (Table 1).

The values of X_{Ep} for studied epidotes range between 0.93 and 1.0 (Mean: 0.97 ±1, Table 1). In addition, they show oscillatory compositional zoning with a very narrow ranges of Fe^{3+}. The Fe^{3+} content of epidote is a function of oxygen fugacity (Spear 1993; Pandit et al. 2014). At oxygen fugacities near the hematite-magnetite buffer, Fe-rich epidote is stable (Bird and Spieler 2004). High Fe^{3+} contents might reflect the high oxygen fugacity during the crystallization of epidote (Spear 1993; Pandit et al. 2014). Therefore, the association of hydrothermal epidote from Varan area with magnetite and hematite and its richness in Fe^{3+}, it confirm that epidote is formed in moderate to high fO_2 conditions.

4.2. FTIR spectral study

The infrared spectrum of the studied epidote is presented in Figure 4 and the assignment and positions of bands are summarized in Table 2. The numeration of the bands is according to Langer and Raith (1974) who

studied the infrared spectral changes within the Al-Fe^{3+} solid solution series as a function of Fe^{3+} content.

Different authors attribute the observed peaks to different modes (Liebscher 2004 and his references). Makreski et al. (2007) briefly presented a review of the vibrational modes for the infrared spectrum of epidote and they assigned the bands 2, 4, 7 ,9, 10 and 11 (1103, 1076, 949, 879, 856 and 833 cm^{-1}, respectively) to the antisymmetric Si-O_{nb} stretching vibrations of the SiO_4 tetrahedra (O_{nb}—non-bridging oxygens) and band 5 (1034 cm^{-1}) to a mixed origin of the Si-O_{nb} stretching modes and OH bending character. The bands 15, 16, 17 and 19 observed at 679, 648,586 and 559 cm^{-1}, respectively, are attributed to Si-O_b-Si bending. The band 8 (902 cm^{-1}) was interpreted as due to an OH bending vibration by Langer and Raith (1974). Because of the complete difference between epidote and clinozoisite spectra in 820–700 and 540-400 cm^{-1}, the bands in these regions are attributed to the M–O vibrations within the various octahedra of the two different structure types (Langer and Raith 1974; Makreski et al. 2007). Thus, the bands 13, 20, 21, 23 and 24 at 714, 540, 513, 462 and 455 cm^{-1}, respectively, arise from Fe^{3+}-O.

Langer and Raith (1974) concluded that in the 200-1200 cm^{-1} region, a number of bands (5, 9, and 13) are resolved as single bands and shift systematically to lower wavenumber with increasing Fe^{3+} in the M3 site. The shift to lower wavenumbers of these bands represented by the linear equation $v = A + Bp$, which can well be used to estimate the Fe^{3+} content of monoclinic epidote Al-Fe^{3+} solid solutions from FTIR spectra, where A is the position of each band at p=0, B the slope of lines and p is Fe^{3+} content on M3 position. The Fe^{3+} content for the studied epidote as calculated is summarized in Table 3.

Table 1. EPMA analyses of epidote from the Varan area with calculations and classifications by using WinEpclas program.

	Ep1-1-c	Ep1-3-m	Ep1-5-r	Ep-2-6-c	Ep2-7-m	Ep2-8-r	Ep-3-9-c	Ep3-10-m	Ep3-11-r
SiO_2	37.71	37.97	36.82	37.56	37.29	36.48	37.72	37.69	37.54
TiO_2	0.24	0.49	0.00	0.06	0.02	0.04	0.06	0.03	0.05
Al_2O_3	21.58	21.51	21.85	22.05	20.98	21.49	21.7	21.27	21.58
Cr_2O_3	0.03	0.00	0.11	0.02	0.00	0.00	0.00	0.00	0.00
FeO (t)	13.71	13.32	14.74	13.59	16.03	15.38	14.43	14.33	14.52
MgO	0.15	0.10	0.03	0.02	0.00	0.04	0.04	0.05	0.02
MnO	0.07	0.08	0.06	0.11	0.12	0.07	0.12	0.19	0.06
CaO	23.64	23.72	23.62	23.66	23.42	23.62	23.41	23.43	23.58
Na_2O	0.05	0.04	0.02	0.04	0.00	0.00	0.05	0.04	0.00
K_2O	0.02	0.02	0.00	0.00	0.00	0.02	0.02	0.00	0.00
Σ (wt%)	97.2	97.25	97.25	97.11	97.86	97.14	97.55	97.03	97.35
Si	3	3.02	2.93	2.99	2.96	2.91	2.99	3.01	2.99
Al^{IV}	0	0	0.07	0.01	0.04	0.09	0.01	0	0.01
Σ T-site	3.00	3.00	3.00	3.00	3.00	3.00	3.00	3.01	3.00
Ti	0.01	0.03	0.00	0.00	0.00	0.00	0.00	0.00	0.00
Al^{VI}	2.02	2.02	1.98	2.06	1.93	1.94	2.02	2.00	2.01
Cr	0.00	0.00	0.01	0.00	0.00	0.00	0.00	0.00	0.00
Fe^{3+}	0.91	0.89	0.98	0.90	1.07	1.03	0.96	0.96	0.97
Mg	0.02	0.01	0.00	0.00	0.00	0.00	0.00	0.01	0.00
Mn^{2+}	0.00	0.00	0.00	0.01	0.00	0.00	0.01	0.01	0.00
ΣM-site	2.97	2.95	2.98	2.98	3.00	2.98	3.00	2.98	2.99
Mn^{2+}	0.00	0.00	0.00	0.00	0.00	0.00	0.00	0.00	0.00
Ca	2.01	2.02	2.02	2.02	1.99	2.02	1.99	2.00	2.01
Na	0.01	0.01	0.00	0.01	0.00	0.00	0.01	0.01	0.00
K	0.00	0.00	0.00	0.00	0.00	0.00	0.00	0.00	0.00
Σ A-site	2.02	2.03	2.02	2.02	2.00	2.02	2.00	2.01	2.01
A1*	Ca	Ca	Ca	Ca	Ca	Ca	Ca	Ca	Ca
A2*	Ca	Ca	Ca	Ca	Ca	Ca	Ca	Ca	Ca
M1*	Al	Al	Al	Al	Al	Al	Al	Al	Al
M2*	Al	Al	Al	Al	Al	Al	Al	Al	Al
M3*	Fe^{3+}	Fe^{3+}	Fe^{3+}	Fe^{3+}	Fe^{3+}	Fe^{3+}	Fe^{3+}	Fe^{3+}	Fe^{3+}
O4&	O	O	O	O	O	O	O	O	O
Subgroup	Clinozoisite	Clinozoisite	Clinozoisite	Clinozoisite	Clinozoisite	Clinozoisite	Clinozoisite	Clinozoisite	Clinozoisite
Name	Epidote	Epidote	Epidote	Epidote	Epidote	Epidote	Epidote	Epidote	Epidote
X_{Ep}	0.97	0.98	0.95	0.93	1.00	0.98	0.97	1.00	0.97

Notes: The formulae were recalculated to 12.5 oxygens and total cations = 8.0; Fe^{3+} and Fe^{2+} estimate from total FeO (wt%) contents; * = Dominant cation; & = Dominant anion; $X_{Ep} = Fe^{3+}/(Fe^{3+}+Al-2)$ of Deer et al. (2013). Abbreviation; c: core; m: mantel; r: rim

The Fe^{3+} calculated from the position of the 5 and 13 bands is 0.94 to 1.07, in line with EPMA data. In addition, compared to the FTIR spectra of epidote with variable Al-Fe^{3+} composition from Langer and Raith (1974), the FTIR bands from this study are in good agreement with corresponding bands related to Fe-rich

epidote (p=0.89). Also, the FTIR spectrum of studied epidote corresponds excellently well with the FTIR spectrum of reference epidote R050303 (Fe^{3+} =0.97) from the RRUFF database (Table 2).

4.3. OH- stretching vibration region

Several publications have adressed the environment of OH in epidote group minerals (e.g., Dollase 1968; Gabe et al. 1973). It was concluded that a H atom is directly bonded to an O10 oxygen which is shared by two adjacent M2 sites. The O10-H form a hydrogen bridge to O4 which is shared by three neighboring M1 M3 M1 sites (Fig. 1b). Therefore, the strength of O–H bond is influenced by the various chemical configurations of the M1M2M3. According to Langer and Raith (1974), epidotes with variable chemical composition (in terms of Al-Fe^{3+}) show a single OH-band, the position of which (wavenumber cm^{-1}) is a linear function of the Fe^{3+} content. They concluded that Fe^{3+} substituting for Al at the M3 octahedral sites causes an increase in the bond strength at the O4 atom (O10-H…O4), which, in turn causes an increase in the position of OH band. With increasing Fe^{3+} content from 0.00 in Clinozoisite to 0.89 in Fe-rich epidote, the position of OH band shifts from 3326 to 3365 cm^{-1}, respectively.

Table 2. Wavenumbers and assignment of the bands in the powder FTIR spectrum of studied epidote, compared with the corresponding literature data.

Band number	This study	Langer and Raith 1974	Makreski et al. 2007	R050303 (Fe^{3+} =0.97)	Tentative assignment
1	3379 vs[a]	3365	3362 vs	3375 vs	*ν*(OH)
2	1103 w	1108	1113 m	1103 w	*ν* (Si-O_{nb})[b]
4	1076 m	1076	1076 m	1072 m	*ν*(Si-O_{nb})
5	1034 m	1035	1038 m	1032 m	*ν*(Si-O_{nb})+δ(OH)
6	-	975 sh	970 sh	-	*ν*(Si-O_{nb})
7	949 vs	951	953 vs	941 vs	*ν*(Si-O_{nb})
8	903 wsh	900 wsh	901 sh	902 wsh	δ(OH)
9	879 s	886	888 s	876 s	*ν*(Si-O_{nb})
10	856 wsh	861	854 vw	856 sh	*ν*(Si-O_{nb})
11	833 w	836	831 w	833 w	*ν*(Si-O_{nb})
12	798 m	800 wsh	-	-	*ν*(M-O)[c]
13	714 w	718	722 w	715 w	*ν*(M-O)
14	694 wsh	697 wsh	-	-	*ν*(M-O)
15	679 sh	670 wsh	673 sh	676 wsh	δ(Si-O_b-Si)
16	648 s	648	646 s	642 s	δ(Si-O_b-Si)
17	586 sh	585 wsh	594 sh	586 wsh	δ(Si-O_b-Si)
19	559 w	563	569 w	555 w	δ(Si-O_b-Si)
20	540 vw	-	539 sh	-	*ν*(M-O)
21	513 s	517	516 s	507 s	*ν*(M-O)
23	462 vw	460 sh	469 sh	461 sh	*ν*(M-O)
24	455 m	454	454 m	449 m	δ(Si-O_b-Si)
25	-	410 wsh	411 sh	407 sh	*ν*(M-O)

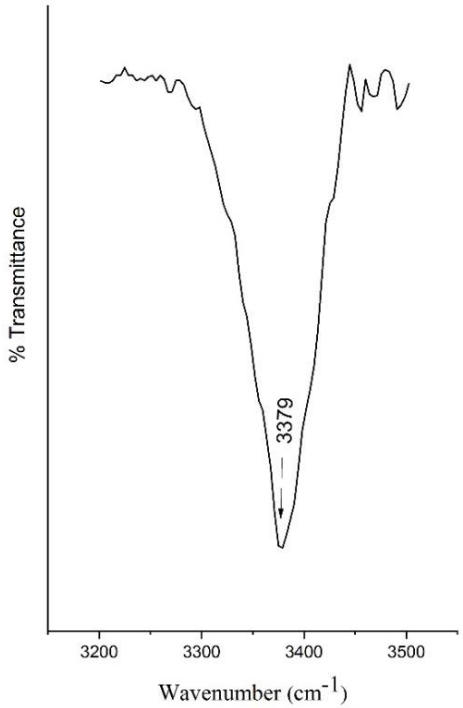

Fig 4. The stretching OH region in the FTIR spectrum of studied epidote.

4.4. Raman study

The Raman spectrum of epidote can be divided into different regions depending upon the type of vibration being activated. The Raman bands presented for studied samples are assigned based on the description proposed in Makreski et al. (2007) and are summarized in Table 4. The bands situated in the wavenumber region 800-1100 cm^{-1} are assigned to symmetric stretching $Si–O_{nb}$ vibrations (from the SiO_4 and Si_2O_7 groups) including the strongest bands at 880 and 909 cm^{-1} for Ep-1 and at 884 and 913 cm^{-1} for Ep-2 (Fig 5). In the 450-750 cm^{-1} spectral region, the main band at 601 cm^{-1} for Ep-1 and at 600 cm^{-1} for Ep-2 is assigned to the symmetric stretching vibrational mode of $Si–O_b–Si$ bonds. The next strong band at 566 cm^{-1} for Ep-1 and at 565 cm^{-1} for Ep-2 is attributed to the $Si–O_b–Si$ bending modes, whereas the medium bands at 500 (Ep-1) and 504 (Ep-2) may be ascribed to the M-O vibrations (M = Fe^{3+} and/or Al in epidote). The bands observed below 300 cm^{-1} probably arise from the external modes (for Ep-1: 90, 138, 167 cm^{-1} and for Ep-2: 90, 132, 167 cm^{-1}).

A comparison between the Raman spectra of the epidote grains (Ep-1 and Ep-2) and two reference samples of epidote from the RRUFF data base are presented in Figure 5, where one of the reference samples has a Fe^{3+} value of 0.64 (R040089) in the M3 site and the other one 0.97 apfu (R050303). The important observation in the Raman bands of the reference samples is the systematic shift toward lower wavenumbers with increasing Fe^{3+} content on the M3 site. The present study reveals that the position of most bands is shifted towards lower frequency as compared to calculated values for the epidote reference spectrum (R040089), which has 0.64 apfu of Fe^{3+} in M3. However, the highest deviation was observed in the stretching vibration of octahedral M sites (300-550 cm^{-1} region). The bands at 345 and 500 cm^{-1} for Ep-1 and at 339 and 504 cm^{-1} for Ep-2 deviated by ~ 10-15 cm^{-1} from the calculated 354 and 515 cm^{-1} wavenumbers for reference epidote with a lower content of Fe^{3+} (0.64 apfu) in the octahedral M3 site, respectively. By comparing the Raman spectra of different reference epidotes (in terms of chemical composition) and Raman spectra of the epidotes analyzed in the present study, we can consider our epidote grains as Fe-rich type, since a similarity is observed between the recorded spectrums and the Raman spectrum of reference epidote with a high content of Fe^{3+} (0.97 apfu) in the octahedral M3 site. However, considering that some peaks registered in our spectrum are intermediate (in terms of bands position) between R050303 and R040089, It might imply that the studied epidote has a composition of Fe^{3+} = 0.8 ±2. This value not very far from the value obtained by EPMA method (mean: Fe^{3+}= 0.958).

Table 3. Fe^{3+} content obtained from the positions of the FTIR bands 1, 5, and 13 by using the linear equation of Langer and Raith (1974).

Band Number	Wavenumbers (ν)	Fe^{3+} content	accuracy
1 (ν OH)	3379	1.1	±0.04
5	1034	0.94	±0.08
13	714	1.07	±0.01

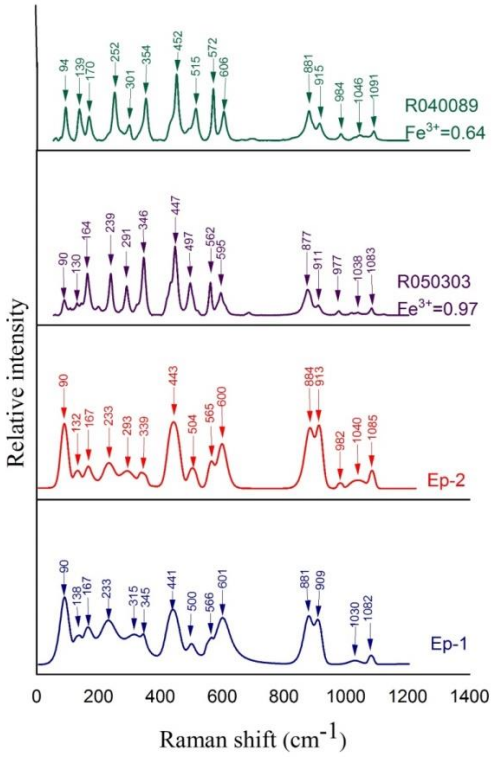

Fig. 5. The μ-Raman spectrum of studied epidote in the 0–1200 cm-1 spectral domain, compared with epidote reference spectra from RRUFF project (with different Fe^{3+} contents).

Table 4. Wavenumbers and assignment of bands observed in the Raman spectra of studied epidote in the 200-1200 cm^{-1} spectral region, in addition to compared the results with epidote reference (R050303 and R040089) spectra from RRUFF project.

This study		R050303 (Fe^{3+} = 0.97)	R040089 (Fe^{3+} = 0.64)	Tentative assignment
Ep-1	Ep-2			
90	90	90	94	-
138	132	130	139	-
167	167	164	170	-
233	233	239	252	-
315	293	291	301	-
345	339	346	354	*ν*(M-O)
441	443	447	452	δ(Si-O_b-Si)
500	504	497	515	*ν*(M-O)
566	565	562	572	δ(Si-O_b-Si)
601	600	595	606	*ν*(Si-O_b)
881	884	877	881	*ν*(Si-O_{nb})
909	913	911	915	*ν*(Si-O_{nb})
-	982	977	984	*ν*(Si-O_{nb})
1030	1040	1038	1046	*ν*(Si-O_{nb})
1082	1085	1083	1091	*ν*(Si-O_{nb})

5. Conclusion

The Fe^{3+} content of epidote obtained by calibrated method of FTIR is in good accordance with those calculated from EPMA data, indicating that studied epidote is closer to pure Fe-epidote. Furthermore, By comparison the Raman spectra for studied epidote with those from the RRUFF database a semi-quantitative (qualitative) estimation of Fe^{3+} content on the M3 site is possible. In this context, it was shown that the application of FTIR to study quantitative chemical composition of epidote is as good as EPMA, whereas the Raman spectroscopy is a fast method and low-cost for qualitative estimation of Fe^{3+} content in epidote.

References

Alavi M (1994) Tectonics of the Zagros orogenic belt of Iran: new data and interpretations. *Tectonophysics* 229: 211–238.

Armbruster T, Bonazzi P, Akasaka M, Bermanec V, Chopin C, Gieré R, Heuss-Assbichler S, Liebscher A, Menchetti S, Pan Y, Pasero M (2006) Recommended nomenclature of Epidote-group minerals. *European Journal of Mineralogy* 18: 551-567.

Baratian M, Arian MA, Yazdi A (2018) Petrology and petrogenesis of the SiahKuh intrusive Massive in the South of KhoshYeilagh, *Amazonia Investiga* 7 (17): 616-629.

Bina M, Arian MA, Pourkermani M, Bazoobandi MH, Yazdi A (2020) Study of the petrography and tectonic settings of sills In Lavasanat district, Tehran (north of Iran), *Nexo Revista Cientifica* 33(2): 286-296.

Bird DK, Spieler AR (2004) Epidote in geothermal systems. Reviews in Mineralogy and Geochemistry, *Mineralogical Society of America* 56: 235-300.

Campos-Alvarez NO, Samson IM, Fryer BJ, Ames DE (2010) Fluid sources and hydrothermal architecture of the Sudbury Structure: Constraints from femtosecond LA-MC-ICP-MS Sr isotopic analysis of hydrothermal Epidote and calcite. *Chemical Geology* 278: 131-150.

Chukanov NV, Göttlicher J, Möckel S, Sofer Z, Van KV, Belakovskiy DI (2010) Åskagenite-(Nd), $Mn^{2+}NdAl_2Fe^{3+}(Si_2O_7)(SiO_4)O_2$, a new mineral of the Epidote supergroup. New Data on Minerals 45: 17-22.

Čobić A (2015) Characterization of metamict minerals with complex crystal-chemical properties–allanite example, PhD thesis, University of Zagreb, 193 p.

Deer WA, Howie RA, Zussman J (2013) An introduction to the rock-forming minerals. The mineralogical society, 3rd Ed., London.

Della Ventura G, Mottana A, Parodi GC, Griffin WL (1996) FTIR spectroscopy in the OH-stretching region of monoclinic Epidotes from Praborna (St. Marcel, Aosta Valley, Italy). *European Journal of Mineralogy* 8: 655-665.

Dollase WA (1968) Refinement and comparison of the structures of zoisite and clinozoisite. American Mineralogist: *Journal of Earth and Planetary Materials* 53: 1882-1898.

Ferreira VP, Sial AN, Pimentel MM, Armstrong R, Spicuzza MJ, Guimarães IP, da Silva Filho AF (2011) Contrasting sources and PT crystallization conditions of Epidote-bearing granitic rocks, northeastern Brazil: O, Sr, and Nd isotopes. *Lithos* 121: 189-201.

Franz G, Liebscher A (2004) Physical and Chemical Properties of the Epidote Minerals–An Introduction–. Reviews in mineralogy and geochemistry, Mineralogical Society of America 56: 1-81.

Freiberger R, Boiron MC, Cathelineau M, Cuney M, Buschaert S (2001) Retrograde P–T evolution and high temperature–low pressure fluid circulation in relation to late Hercynian intrusions: a mineralogical and fluid inclusion study of the Charroux-Civray plutonic complex (north-western Massif Central, France). *Geofluids* 1: 241-256.

Gabe EJ, Portheine JC, Whitlone SH (1973) A reinvestigation of the epidote structure: confirmation of the iron location. American Mineralogist: *Journal of Earth and Planetary Materials* 58: 218-223.

Gavorkyan SV (1990) IR spectra of Epidote-group minerals. Mineralogiceskij zurnal 12: 63-66 (in Russian).

Ghalamghash J, Babakhani AR (1996) Geological Map of Kahak: Geological Survey of Iran, Scale 1:100000 Sheet.

Gieré R, Sorensen SS (2004) Allanite and other REE-rich Epidote-group minerals. Reviews in Mineralogy and Geochemistry, Mineralogical Society of America 56: 431-493.

Huang E (1999) Raman spectroscopic study of 15 gem minerals. *Journal of the Geological Society of China* 42: 301-318.

Janeczek J, Sachanbinski M (1989) Chemistry and zoning of thulite from the Wiry magnesite deposit, Poland. Neues Jahrbuch Fur Mineralogie-Monatshefte 7: 325-333.

Khademi Parsa M (2017) Petrology of ore related intrusive and subvolcanic rocks and their aureoles in NE Delijan (Urumieh-Dokhter magmatic arc). Ph.D. thesis, Department of Minerals & Groundwater Resources, Faculty of Earth Sciences, Shahid Beheshti University, Tehran, Iran.

Klemd R (2004) Fluid inclusions in Epidote minerals and fluid development in Epidote bearing rocks. Reviews in mineralogy and geochemistry 56: 197-234.

Langer K, Raith M (1974) Infrared spectra of Al-Fe (III)-Epidotes and zoisites, Ca_2 (Al1-p Fe^{3+}p) Al_2O (OH)[Si_2O_7][SiO_4]. American Mineralogist: *Journal of Earth and Planetary Materials* 59: 1249-1258.

Liebscher A (2004) Spectroscopy of epidote minerals. Reviews in Mineralogy and Geochemistry 56: 125-170.

Makreski P, Jovanovski G, Kaitner B, Gajović A, Biljan T (2007) Minerals from Macedonia: XVIII. Vibrational spectra of some sorosilicates. Vibrational Spectroscopy 44: 162-170.

McFarlane CR (2016) Allanite UPb geochronology by 193 nm LA ICP-MS using NIST610 glass for external calibration. Chemical Geology 438: 91-102.

Mingsheng P, Dien L (1987) Spectroscopy, genesis, and process properties of partly metamict allanite. J Central-South Inst Mining Metall 18: 362-368.

Pandit D, Panigrahi MK, Moriyama T (2014) Constrains from magmatic and hydrothermal Epidotes on crystallization of granitic magma and sulfide mineralization in Paleoproterozoic Malanjkhand Granitoid, Central India. *Geochemistry* 74: 715-733.

Perseil EA (1987) Particularités des piémontites de Saint-Marcel-Praborna (Italie); spectres IR. *Congrès National des Sociétés Savantes* 112: 209-215 (in French).

Petrusenko S, Taran MN, Platonov AN, Gavorkyan SV (1992) Optical and infrared spectroscopic studies of Epidote group minerals from the Rhodope region. Spisanie na B ″lgarskoto geologičesko družestvo 53: 1-9.

Sarem MN, Abedini MV, Dabiri R, Ansari MR (2021) Geochemistry and petrogenesis of basic Paleogene volcanic rocks in Alamut region, Alborz mountain, north of Iran. *Earth Sciences Research Journal* 25(2):237-45.

Spear FS (1993) Metamorphic Phase Equilibria and Pressure-Temperature-Time Paths. Mineralogical Society of America, Washington 60:992-3.

Varlamov DA, Ermolaeva VN, Chukanov NV, Jančev S, Vigasina MF, Plechov PY (2019) New data on chemical composition and Raman spectra of Epidote-supergroup minerals. In Proceedings of the Russian Mineralogical Society 148: 79-99.

Whitney DL, Evans BW (2010). Abbreviations for names of rock-forming minerals. American Mineralogist 95: 185–187.

Yavuz F, Yildirim DK (2018) A Windows program for calculation and classification of Epidote-supergroup minerals. Periodico di Mineralogia 87: 269-285.

Yazdi A, Shahhosseini E, Moharami F (2022) Petrology and tectono-magmatic environment of the volcanic rocks of West Torud–Iran, *Iranian Journal of Earth Sciences* 14(1): 40-57.